Critical filling factor for the formation of a quantum Wigner crystal screened by a nearby layer

H. Deng, L. W. Engel, L. N. Pfeiffer, K. W. West, K. W. Baldwin, and M. Shayegan

Critical Filling Factor for the Formation of a Quantum Wigner Crystal Screened by a Nearby Layer

H. Deng, L.N. Pfeiffer, K.W. West, K.W. Baldwin, and M. Shayegan

Department of Electrical Engineering, Princeton University

(Dated: August 1, 2018)

One of the most fascinating ground states of an interacting electron system is the so-called Wigner crystal where the electrons, in order to minimize their repulsive Coulomb energy, form an ordered array. Here we report measurements of the critical filling factor (ν_C) below which a magnetic-field-induced, quantum Wigner crystal forms in a dilute, two-dimensional electron layer when a second, high-density electron layer is present in close proximity. The data reveal that the Wigner crystal forms at a significantly smaller ν_C compared to the ν_C ($\simeq 0.20$) in single-layer two-dimensional electron systems. The measured ν_C exhibits a strong dependence on the interlayer distance, reflecting the interaction and screening from the adjacent, high-density layer.

When the Coulomb energy (E_C) in an interacting electron system dominates over the kinetic energy, it has long been expected that the system condenses into a Wigner crystal (WC) where electrons order themselves in a periodic lattice [1]. A *classical* WC state was indeed realized in a very dilute two-dimensional electron system (2DES) confined to the surface of liquid He at sufficiently low temperatures when E_C dominates the kinetic (thermal) energy [2, 3]. At higher densities, the Fermi energy becomes large and plays the role of the kinetic energy; in this case a *quantum* WC can be stabilized if E_C is much larger than the Fermi energy [4] and temperature is sufficiently low. The addition of a strong, quantizing, perpendicular magnetic field facilitates the formation of a quantum WC as it quenches the kinetic energy by forcing the electrons into the lowest Landau level (LL) [5–7]. Such a magnetic-field-induced WC has been studied using various experimental techniques in very high mobility (low-disorder) 2DESs confined to modulation-doped GaAs quantum wells [8–16]. The measurements have established that, at LL filling factors ν smaller than $\simeq 0.20$, there is an insulating phase which is generally interpreted to signal the formation of a WC pinned by the small but ubiquitous disorder potential. In very low-disorder GaAs 2DESs, the WC correlation lengths deduced from the measurements are typically much larger than the WC lattice constant, implying large domains and long-range spatial order [12].

Here we address a general and fundamental question: What happens to the WC if one brings a second layer in close proximity; in particular, how does such a layer modify the Coulomb interaction in the WC layer? In the case of a classical 2D WC, theory [17, 18] and experiments [19] indicate that placing a conductive plate below the thin liquid He film on which the 2D WC is formed screens the Coulomb interaction and weakens the stability of the WC. In order to boost the ratio of the Coulomb to the thermal energy and re-stabilize the WC, higher electron densities and/or lower temperatures are needed [17–19]. The role of screening on a quantum WC, however has not been studied so far. In our study we probe the stability of the magnetic-field-induced, quantum WC at very low temperatures in carefully-designed, bilayer electron systems (BLESs) with very asymmetric layer densities. The majority-density layer acts as the screening layer, and influences the critical LL filling factor (ν_C) below which the WC forms in the minority layer. Our measured ν_C in BLESs with different interlayer distances reveal that, if the screening layer is close by ($\simeq 40$ nm), ν_C can be reduced by more than an order of magnitude compared to the $\nu_C \simeq 0.20$ for a single-layer 2DES. This observation implies that, for a *quantum* WC, the weakening of the Coulomb interaction caused by a screening layer shifts ν_C (or, equivalently the critical density below which the WC forms) to smaller values. Our systematic measurements of ν_C and its dependence on the interlayer distance and other parameters of the BLES provide unique data which should stimulate quantitative, rigorous calculations.

Our samples are grown via molecular beam epitaxy and contain two 30-nm-wide GaAs quantum wells (QWs), separated by varying thicknesses of $Al_{0.24}Ga_{0.76}As$ barriers: 10 nm for samples A and B, 20 nm for sample C, and 50 nm for samples D and E. The QWs are modulation-doped with Si δ-layers asymmetrically. As grown, the majority- and minority-layer densities near zero magnetic field (B) are $n_{Maj,0} \simeq 1.45$ and $n_{Min,0} \simeq 0.45$, in units of 10^{11} cm^{-2} which we use throughout the manuscript. Samples A, C, and D have the majority layer on the top and minority layer on the bottom, while samples B and E have an inverted layer order. All the samples have a van der Pauw ($\simeq 4 \times 4$ mm^2) geometry, except for sample A which is a 200×800 μm^2 Hall bar. We use In-Sn alloy to make Ohmic contacts to both layers. Top and bottom gates are fabricated to tune each layer's density. In order to measure the longitudinal (R_{xx}) and Hall (R_{xy}) resistance, we use low-frequency (≤ 30 Hz) lock-in technique and a dilution refrigerator with a base temperature of $\simeq 30$ mK.

In Fig. 1, we demonstrate our determination of the WC density (n_{WC}) and ν_C using data for sample A. Near $B = 0$, we measure $n_{Maj,0}$ and $n_{Min,0}$ from the Fourier transform of the low-field Shubnikov-de Haas oscillations. The sum of $n_{Maj,0}$ and $n_{Min,0}$ gives the total density, which we assume remains constant as a function
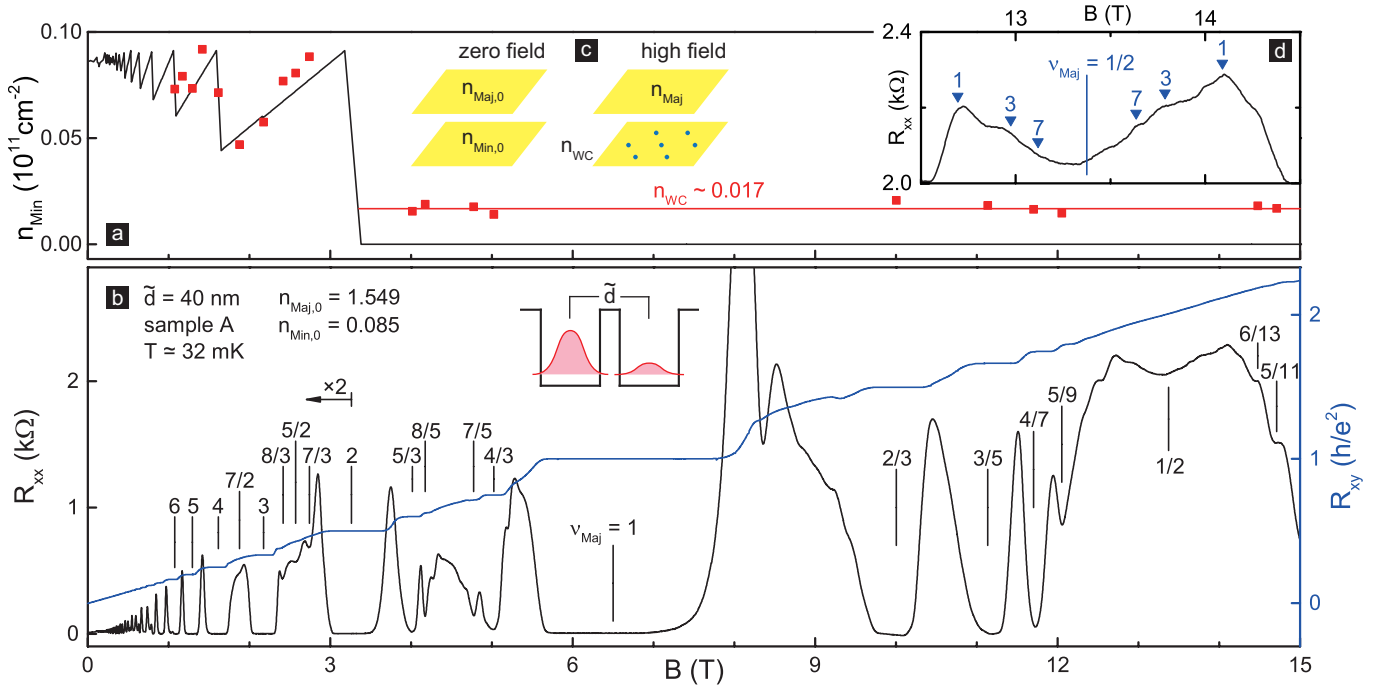
FIG. 1. (a) The evolution of minority layer density (n_{Min}) with magnetic field for sample A. Black lines represent the calculated values based on the LLA model with the zero-field layer densities ($n_{Maj,0}$ and $n_{Min,0}$) and the interlayer distance as inputs. Red squares are the measured n_{Min}. Red horizontal line indicates the WC density (n_{WC}) determined by averaging the measured n_{Min} at high B (> 3.3 T). (b) Magnetotransport traces for sample A: R_{xx} (black), and R_{xy} (blue). The filling factors for the majority layer (ν_{Maj}) are noted for the main QHSs and the half fillings. The R_{xx} trace for $B < 3.3$ T is amplified by a factor of 2 for clarity. The inset is a diagram for the double-QW sample structure, showing the definition of the center-to-center distance ($\tilde{d}$). (c) Diagram showing the state of each layer at $B = 0$ and high B. (d) Details of R_{xx} near $\nu_{Maj} = 1/2$. Blue triangles indicate the expected positions of the commensurability maxima based on the measured n_{WC}. The numbers above the triangles indicate the number of WC lattice points encircled by the composite fermions' cyclotron orbits [15].

of B even at the largest B. Using $n_{Maj,0}$, $n_{Min,0}$, and the center-to-center distance $\tilde{d}$ (the sum of the barrier thickness and QW width; see Fig. 1(b) inset) as inputs, we apply a Landau level alignment (LLA) model to calculate the evolution of the layer densities as a function of B [20, 21]. The LLA model considers the fact that applying B induces LLs in each layer, and that thermal equilibrium requires the Fermi levels to be the same in both layers. As a consequence, the evolution of the LLs in each layer changes the interlayer potential, and induces an interlayer charge transfer [20, 21].

We plot in Fig. 1(a) (black curve) the calculated B-dependence of the minority-layer density (n_{Min}) based on the LLA model. Experimentally, we measure the majority-layer density (n_{Maj}) as a function of B from the positions of the quantum Hall states (QHSs), namely the minima of the R_{xx} trace in Fig. 1(b) [25]. Because of the much higher n_{Maj}, the R_{xx} minima at intermediate and high B reflect the QHSs of the majority layer [15, 20]. By subtracting n_{Maj} from the total density, we deduce n_{Min} as a function of B and plot the data as red squares in Fig. 1(a). The calculated n_{Min} matches the experimental values reasonably well in the intermediate B regime where the majority-layer filling factor $\nu_{Maj} > 2$, but at higher B

where $\nu_{Maj} < 2$, there is a noticeable difference between the calculated and experimental values. The calculation predicts the complete depletion of the minority layer following a large charge transfer at $\nu_{Maj} = 2$. However, the measured n_{Min} attains a finite, constant value up to the highest B [red horizontal line in Fig. 1(a)].

We attribute the residual n_{Min} at high B to the formation of a WC in the minority layer. Starting with certain $n_{Maj,0}$ and $n_{Min,0}$ [Fig. 1(c)], as a function of B electrons freely transfer between the layers, consistent with the LLA model. At high B (> 3.3 T), when n_{Min} is sufficiently low so that the minority-layer filling factor (ν_{Min}) is very small, the WC in the minority layer becomes energetically favored and terminates the charge transfer because a pinned WC is essentially incompressible. Note that n_{Min} remains constant for $B > 3.3$ T, consistent with the formation of an incompressible WC [26]. This is further corroborated by our observation of commensurability oscillations (COs) which support the existence of the WC [Fig. 1(d)]. Near $\nu_{Maj} = 1/2$, the majority-layer electrons form composite fermions (CFs) and execute cyclotron motion in the effective magnetic field [27–29]. If the CFs feel a periodic electric potential modulation from a WC layer in close proximity, R_{xx}
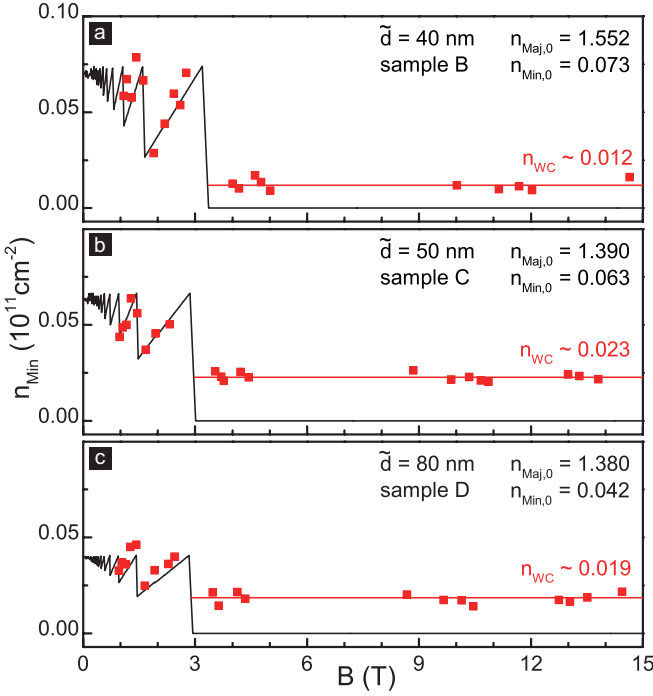
FIG. 2. (a)-(c) The evolution of n_{Min} with B for samples with $\widetilde{d} = 40$, 50 and 80 nm. In each panel, the black curve is the calculated value of n_{Min}, red squares are the measured n_{Min}, and red horizontal line indicates the value of n_{WC}.

exhibits maxima whenever the CFs' cyclotron orbits encircle a certain integer number of the WC lattice points [15]. In Fig. 1(d), the blue triangles mark the expected positions of COs based on the modulation from the WC with the density $n_{WC} \simeq 0.017$. The reasonable agreement between the expected and measured positions of R_{xx} maxima supports the existence of the WC.

The phenomena observed in Fig. 1 is qualitatively seen in our other samples, as illustrated in Fig. 2. Here we show the calculated and measured values of n_{Min} for samples B, C and, D, which have $\widetilde{d}$ equal to 40, 50, and 80 nm, respectively. In all three panels, we start with a sufficiently low $n_{Min,0}$, and the calculation based on the LLA model predicts a complete depletion of the minority layer for *all* the samples at high B when $\nu_{Maj} < 2$. However, the measurements show that the minority layer retains a fraction of electrons in the high-B regime. The data indicate that the retainment of the electrons in the minority layer at high B is a general property of the asymmetric BLESs. As described in the preceding paragraph, we attribute the retained electrons to the formation of a WC with density n_{WC} in the minority layer.

The value of n_{WC} for a given initial $n_{Min,0}$ directly reflects the impact of the adjacent, majority layer. In Fig. 3(a), we plot the measured n_{WC} against $n_{Min,0}$ for all the samples. For each sample, we make measurements for multiple values of $n_{Min,0}$ which we tune by applying voltage bias to the gate near the minority layer. Despite the scatter and the measurement error bars, the data

in Fig. 3(a) reveal a clear dependence on $\widetilde{d}$: For a fixed $n_{Min,0}$, n_{WC} increases with increasing $\widetilde{d}$. Moreover, for a given $\widetilde{d}$, n_{WC} shows an approximately linear dependence on $n_{Min,0}$. We would like to point out that $n_{Maj,0}$ varies slightly for different samples even though the wafers were designed to have the same density. Moreover, because of negative compressibility [24, 30–32], $n_{Maj,0}$ also changes when we use the gate bias to tune $n_{Min,0}$. In the range of our experiments, the overall variation of n_{Maj}, is $\simeq 10\%$ (see, e.g. $n_{Maj,0}$ listed in Figs. 1 and 2). To appraise the role of $n_{Maj,0}$, we also made a full batch of measurements on sample B ($\widetilde{d} = 40$ nm) with $\simeq 20\%$ lower $n_{Maj,0}$ by applying bias to the gate near the majority layer; the results are plotted as black triangles in Fig. 3(a). As seen in Fig. 3(a), the triangles lie only very slightly above the other black data points, suggesting a weak dependence on $n_{Maj,0}$; we will return to the role of $n_{Maj,0}$ later in the manuscript.

To further summarize the dependence on $\widetilde{d}$ demonstrated in Fig. 3(a), we apply a least-squares linear fit to each group of data belonging to different $\widetilde{d}$, and plot the slopes ($dn_{WC}/dn_{Min,0}$) of the fitted lines against $1/\widetilde{d}$ in Fig. 3(b) [33]. Moreover, for each data point in Fig. 3(a), we use n_{WC} and the B value at $\nu_{Maj} = 2$, above which the interlayer charge transfer stops, to determine the ν_C for the formation of the WC. Figure 3(d) contains a plot of ν_C from all our measurements. In Fig. 3(c), we show a subset of this data, namely ν_C for a fixed $n_{Min,0} = 0.07$, plotted as a function of $1/\widetilde{d}$ [34].

Figure 3(b) reveals the tendency that, the larger $\widetilde{d}$ is, the larger the fraction of electrons that stay in the minority layer and form a WC. At the same time, Fig. 3(c) demonstrates that, the larger $\widetilde{d}$ is, the larger ν_C of the minority-layer WC. Both figures help portray the impact of the majority layer on the WC formed in the minority layer. In the case of small $\widetilde{d}$ [e.g., $\widetilde{d} = 40$ nm in Figs. 3(b) and 3(c)], the nearby majority layer significantly screens the Coulomb interaction between the minority-layer electrons. With a weaker Coulomb interaction, the minority-layer electrons need a smaller ν_C for the WC to achieve the dominance of E_C over the kinetic energy. As a consequence, a smaller fraction of electrons are retained as WC in the minority layer. In the case of large $\widetilde{d}$ [e.g., $\widetilde{d} = 50$ and 80 nm in Figs. 3(b) and 3(c)], the screening by the majority layer becomes less significant, and the Coulomb interaction between minority-layer electrons becomes stronger, resulting in a larger ν_C and larger fraction of retained electrons. Note that, in the limit of infinite $\widetilde{d}$, the minority layer is in effect a single-layer 2DES, and all the minority-layer electrons should remain in this layer and form a WC at $\nu_C \simeq 0.2$ [open symbols in Figs. 3(b) and (c)]. The data in Figs. 3(b) and (c) indeed show an asymptotic behavior toward the expected value in the limit of infinite $\widetilde{d}$.

In Fig. 3(d), we plot ν_C from all the measurements against a dimensionless parameter $\alpha = 1/(\widetilde{d} \times n_{WC}^{1/2})$ in
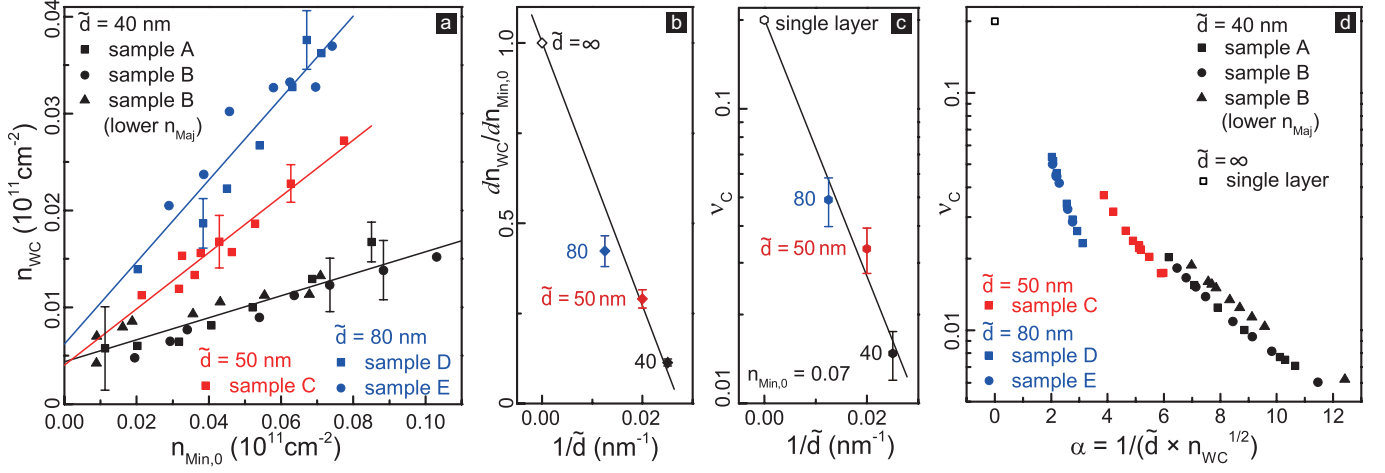
FIG. 3. (a) The measured n_{WC} as a function of $n_{Min,0}$. The black, red, and blue points are data from samples with $\widetilde{d} = 40$, 50 and 80 nm, respectively. Typical error bars are given, and the straight lines are the least-squares linear fits for different groups of data. (b) The slopes of the linear fits in (a) as a function of $1/\widetilde{d}$. The expected limit of $dn_{WC}/dn_{Min,0}$ at $\widetilde{d} = \infty$ is equal to unity and is plotted by an open symbol. The black line is a guide to eye. (c) ν_C as a function of $1/\widetilde{d}$ at fixed $n_{Min,0} = 0.07$. The error bars include the uncertainty of both n_{WC} and the field position above which the charge transfer stops near $\nu_{Maj} = 2$ in Figs. 1(a) and 2]. The limit of ν_C for the WC in single-layer 2DES (0.20) is plotted at $1/\widetilde{d} = 0$ as a reference. The line is drawn to guide the eye. (d) ν_C as a function of a dimensionless parameter α. The limit of ν_C for the WC in a single-layer 2DES (0.20) is plotted at $\alpha = 0$ as a reference.

an attempt to quantify the impact of the screening by the adjacent majority layer. Intuitively, the smaller $\widetilde{d}$ is, the stronger the screening, leading to a smaller ν_C for the formation of WC because the intralayer Coulomb interaction in the minority layer is further weakened. Considering that the intralayer Coulomb interaction in the minority layer is determined by the electrons' average distance $r \propto 1/n_{WC}^{1/2}$, we compare $\widetilde{d}$ and r, and use their ratio ($\alpha = r/\widetilde{d}$) to characterize the screening. In Fig. 3(d), we also plot $\nu_C \simeq 0.20$ for the WC in a single-layer 2DES at $\alpha = 0$ as a reference. Overall, the data from all the samples with varying $\widetilde{d}$ and n_{WC} generally follow the same tendency toward the limit of single-layer 2DES, indicating the effect of screening on the formation of WC.

The data of sample B with $\simeq 20\%$ lower $n_{Maj,0}$ [black triangles in Fig. 3(d), $n_{Maj,0} \simeq 1.30$] show slightly higher ν_C compared to the data of sample B with larger $n_{Maj,0}$ (black circles, $n_{Maj,0} \simeq 1.56$). According to the Thomas-Fermi approximation, the screening efficiency in a 2DES is independent of the layer density [35], so ν_C of sample B should be the same for different $n_{Maj,0}$. However, previous studies of negative compressibility demonstrate that, in an interacting BLES, the screening of one layer by another depends on the layer densities [24, 30–32]. This interaction-induced, density-dependent screening beyond

the Thomas-Fermi approximation might be responsible for our observation of the dependence of ν_C on $n_{Maj,0}$.

In conclusion, our measurements in multiple, asymmetric BLESs with small minority-layer densities reveal that the formation of a magnetic-field induced WC at high magnetic fields retains electrons in this layer and terminates the interlayer charge transfer. Moreover, we find that the critical filling factor ν_C for WC formation strongly depends on the interlayer distance and is significantly lower than ν_C for a single-layer WC, reflecting the interlayer interaction and screening from the adjacent, majority layer. We hope that our systematic and quantitative data, summarized in Fig. 3, would inspire rigorous theoretical work on the physics of a quantum WC under the impact of screening by a nearby layer.

[1] E. Wigner, Phys. Rev. **46**, 1002 (1934).

[2] C. C. Grimes and G. Adams, Phys. Rev. Lett. **42**, 795

(1979).

[3] D. S. Fisher, B. I. Halperin, and P. M. Platzman, Phys. Rev. Lett. **42**, 798 (1979).

[4] J. Yoon, C. C. Li, D. Shahar, D. C. Tsui, and M. Shayegan, Phys. Rev. Lett. **82**, 1744 (1999).

[5] Y. E. Lozovik and V. I. Yudson, JETP Lett. **22**, 11 (1975).

[6] P. K. Lam and S. M. Girvin, Phys. Rev. B **30**, 473 (1984).

[7] D. Levesque, J. J. Weis, and A. H. MacDonald, Phys. Rev. B **30**, 1056 (1984).

[8] E. Y. Andrei, G. Deville, D. C. Glattli, F. I. B. Williams, E. Paris, and B. Etienne, Phys. Rev. Lett. **60**, 2765 (1988).

[9] H. W. Jiang, R. L. Willett, H. L. Stormer, D. C. Tsui, L. N. Pfeiffer, and K. W. West, Phys. Rev. Lett. **65**, 633 (1990).

[10] V. J. Goldman, M. Santos, M. Shayegan, and J. E. Cunningham, Phys. Rev. Lett. **65**, 2189 (1990).

[11] Y. P. Li, T. Sajoto, L. W. Engel, D. C. Tsui, and M. Shayegan, Phys. Rev. Lett. **67**, 1630 (1991).

[12] P. D. Ye, L. W. Engel, D. C. Tsui, R. M. Lewis, L. N. Pfeiffer, and K. West, Phys. Rev. Lett. **89**, 176802 (2002).

[13] Y. P. Chen, G. Sambandamurthy, Z. Wang, R. Lewis, L. Engel, D. Tsui, P. Ye, L. Pfeiffer, and K. West, Nat. Phys. **2**, 452 (2006).

[14] L. Tiemann, T. D. Rhone, N. Shibata, and K. Muraki, Nat. Phys. **10**, 648 (2014).

[15] H. Deng, Y. Liu, I. Jo, L. N. Pfeiffer, K. W. West, K. W. Baldwin, and M. Shayegan, Phys. Rev. Lett. **117**, 096601 (2016).

[16] For an early review, see M. Shayegan, "Case for the Magnetic-field-induced Two-dimensional Wigner Crystal", in *Perspectives in Quantum Hall Effects*, edited by S.D. Sarma and A. Pinczuk (Wiley, New York, 1997), pp. 343-383.

[17] F. M. Peeters and P. M. Platzman, Phys. Rev. Lett. **50**, 2021 (1983).

[18] F. M. Peeters, Phys. Rev. B **30**, 159 (1984).

[19] G. Mistura, T. Günzler, S. Neser, and P. Leiderer, Phys. Rev. B **56**, 8360 (1997).

[20] H. Deng, Y. Liu, I. Jo, L. N. Pfeiffer, K. W. West, K. W. Baldwin, and M. Shayegan, Phys. Rev. B **96**, 081102 (2017).

[21] See Supplemental Material for details of the LLA model, which includes Refs. [20, 22–24].

[22] A. G. Davies, C. H. W. Barnes, K. R. Zolleis, J. T. Nicholls, M. Y. Simmons, and D. A. Ritchie, Phys. Rev. B **54**, R17331 (1996).

[23] Y. Liu, J. Shabani, D. Kamburov, M. Shayegan, L. N. Pfeiffer, K. W. West, and K. W. Baldwin, Phys. Rev. Lett. **107**, 266802 (2011).

[24] X. Ying, S. R. Parihar, H. C. Manoharan, and M. Shayegan, Phys. Rev. B **52**, R11611 (1995).

[25] In order to show QHSs in the low-field regime ($B < 3.3$ T) clearly in Fig. 1(b), we present the R_{xx} trace from another high-quality sample in van der Pauw geometry, which has the same $n_{Maj,0}$, $n_{Min,0}$, and $\widetilde{d}$.

[26] Data in Fig. 2(a) of Ref. [20] corroborate our conjecture: When the minority layer has high density so it does not form a WC and is therefore in a *compressible* state, the interlayer charge transfer continues in the high-field regime of $\nu_{Maj} < 2$.

[27] J. K. Jain, Phys. Rev. Lett. **63**, 199 (1989).

[28] B. I. Halperin, P. A. Lee, and N. Read, Phys. Rev. B **47**, 7312 (1993).

[29] J. K. Jain, *Composite Fermions* (Cambridge University Press, Cambridge, UK, 2007).

[30] J. P. Eisenstein, L. N. Pfeiffer, and K. W. West, Phys. Rev. B **50**, 1760 (1994).

[31] Y. Katayama, D. Tsui, H. Manoharan, and M. Shayegan, Surface Science **305**, 405 (1994).

[32] S. J. Papadakis, J. P. Lu, M. Shayegan, S. R. Parihar, and S. A. Lyon, Phys. Rev. B **55**, 9294 (1997).

[33] Because the exact form for the dependence of n_{WC} on $n_{Min,0}$ is unknown, we use the linear fit as a simple approximation. The positive intercepts of the linear fits might originate from the deviation between the linear approximation and the exact form, or the error bar of the experimental data points, or both.

[34] Converting data at other values of $n_{Min,0}$ in Fig. 3(a) to ν_C and plotting them as in Fig. 3(c) leads to qualitatively similar behavior. Figure 3(d) provides a complete set of ν_C values deduced for all the data points of Fig. 3(a).

[35] J. H. Davies, *The Physics of Low-dimensional Semiconductors* (Cambridge University Press, Cambridge, UK, 1998).